To be published in Astrophysics Journal Letters
Preprint typeset using LaTeX style emulateapj v. 12/14/05

CHANDRA/HETGS OBSERVATIONS OF THE CAPELLA SYSTEM: THE PRIMARY AS A DOMINATING X-RAY SOURCE

Kazunori Ishibashi, Daniel Dewey, David P. Huenemoerder, and Paola Testa
Massachusetts Institute of Technology Kavli Institute for Astrophysics and Space Research, 77 Massachusetts Ave. Cambridge, MA 02139

To be published in Astrophysics Journal Letters

ABSTRACT

Using the *Chandra*/High Energy Transmission Grating Spectrometer (hereafter HETGS) we have detected Doppler motion of Capella's X-ray emission lines in the 6 – 25Å wave-band. The observed motion follows the expected orbital motion of Capella's primary. This finding implies that the primary G8 III star, not the secondary G1 III star in the Hertzsprung gap, has been the dominant source of hot $10^{6.8}$ – 10^7 K plasma at least in the last six years. In addition, the results demonstrate the long-term stability of the HETGS and demonstrate small uncertainties of 25 and 33 km s^{-1} in the velocity determination with the HEG and MEG, respectively.

Subject headings: stars: late-type — binaries: spectroscopic — stars: individual(Capella) — stars: evolution — X-rays: stars

1. INTRODUCTION

Capella (α Aurigae = HD 34029, $\alpha = 5^h\ 16^m\ 41.4^s$, $\delta = 45^\circ\ 59'\ 53''$ in Epoch 2000.0) is a well-studied binary system consisting mainly of two cool giants: G8 III and G1 III (often labeled as Aa and Ab, respectively). The two giants have very similar masses of 2.69 and 2.56 $M_\odot$ (Hummel et al. 1994)[1]. The cooler, more massive G8 III star is a core He-burning (CHeB) clump giant, while the hotter secondary G1 III star is a rapidly rotating giant crossing the Hertzsprung gap for the first time (Pilachowski & Sowell 1992; Barlow, Fekel, & Scarfe 1993 and references therein). Generally both gap and clump stars show hot ($T \sim 10^7$K) coronal emission measure distribution, although gap stars are often found more deficient in X-rays than clump stars (Ayres et al. 1998).

In the case of the Capella system, it was not clear how much each star contributed to the total X-ray luminosity. Linsky et al. (1998) found that the contribution of the G8 star to the total Fe XXI λ1354 flux (forming at T $\sim$ 10^7K) equaled that of the G1 star in the 1995 and 1996 observations with the *Hubble Space Telescope*/Goddard High-Resolution Spectrometer, whereas the G8 star contributed less in other UV lines forming at much lower temperatures. Johnson et al. (2002), instead, found in 1999 with the *HST*/Space Telescope Imaging Spectrograph that the G8 star exhibited a negligible contribution to the same line, indicating that the 10^7K plasma of the G8 star was variable on a long time scale. In contrast to the finding by Johnson et al., Young et al. (2001) found in 2000 with the *Far Ultraviolet Spectroscopic Explorer* that the Fe XVIII λ974.85 line (forming at T $\sim$ $10^{6.8}$K) originated mainly from the G8 star. Since the emission measure distribution of Capella sharply peaked at T $\sim$ $10^{6.8}$K (Brickhouse et al. 2000; Ness et al. 2003; Argiroffi et al. 2003; and references therein), it seemed natural to expect that the main contribution to Capella's X-ray emission originated from the G8 star. However, it was not proven definitively.

To date, no X-ray telescope can resolve these stars spatially (separation $\approx 0.06''$; c.f., Young et al. 2002 on spatially separating the two giants in the UV with the *HST*/Faint Object Camera). However, a definitive determination of the origin of Capella's hard X-rays can be achieved by following the Doppler motion of bright emission lines in the observed *Chandra*/HETG spectra in its six years' operation.

2. OBSERVATIONS AND DATA PROCESSING

Capella has been observed 14 times (see Table 1) in the Timed Event (TE) mode with the *Chandra*/HETGS (Canizares et al. 2005) for purposes of calibration and data collection for the Emission Line Project[2].

Each dataset was obtained through the Chandra X-ray Center data archive and was reprocessed with the CIAO tools (version 3.2.1); and ancillary effective area and grating line response products were generated with the CALDB 3.0.1. The reprocessing included the latest updates on the ACIS-S chip geometry and the MEG grating period[3]. No pixel randomization in the output of `tg_resolve_events` was added and the default CIAO extraction settings were applied.

Since the Capella system is a modestly bright X-ray source (photon flux $f_X \approx 2$ cps at 0^{th} order image in the HETG wave-band), its 0^{th} order image is piled up. This leads to poor determination of the centroid peak in the 0^{th} order image and hence a poorer zero-wavelength solution. To remedy this, the 0^{th} order position was re-derived based on the intersection of the grating arms and the 0^{th}-order ACIS frame transfer streak.

3. LINE ANALYSIS

To determine accurate Doppler velocities of the bright emission lines in the Capella spectrum, we followed this procedure: (1) select a region of Capella's spectrum containing strong emission lines; (2) fit the line position of

Electronic address: bish@space.mit.edu

[1] It makes little difference in the following work if the mass values by Barlow et al.(1993) are quoted, instead.

[2] http://cxc.harvard.edu/elp/ELP.html

[3] http://space.mit.edu/CXC/docs/docs.html#acis_s_geom

TABLE 1
Chandra/HETGS Observations of Capella

ObsID	Date Start (MJD)	Good Time Interval (ksec)	Phase ϕ	Apparent Velocity V_{obs}	Apparent Velocity 3σ confidence (km/s)	Corrected Radial Velocity (V_{bary} km/s)	Barycenter Correction (C_{bary} km/s)	Spacecraft Velocity (C_{sc} km/s)
1099	51418.329	14.6	0.398	−34.9	(−19.3 ∼ −52.7)	−8.65	26.0	0.214
1235	51418.512	14.6	0.400	−25.3	(−7.77 ∼ −41.7)	0.97	26.0	0.272
1100	51418.694	14.6	0.402	−10.0	(+8.94 ∼ −29.5)	16.4	26.1	0.325
1236	51418.877	14.6	0.404	−13.2	(+6.31 ∼ −34.6)	13.3	26.1	0.375
1101	51419.060	14.6	0.405	−16.3	(+4.25 ∼ −32.2)	10.2	26.1	0.420
1237	51419.243	14.6	0.407	−15.0	(+5.01 ∼ −32.2)	11.6	26.1	0.451
1103	51445.257	40.5	0.657	−6.92	(+3.04 ∼ −16.4)	20.4	26.9	0.392
1318	51446.560	26.7	0.670	−10.2	(+4.37 ∼ −24.4)	16.4	26.8	−0.182
0057	51606.687	28.8	0.209	67.4	(+80.1 ∼ +54.7)	40.4	−27.3	0.352
1010	51951.516	29.5	0.524	26.2	(+42.7 ∼ +16.2)	1.57	−24.2	−0.468
2583	52393.741	27.6	0.775	54.6	(+68.1 ∼ +44.6)	35.4	−18.8	−0.485
3674	52909.818	28.7	0.736	−4.34	(+9.86 ∼ −17.1)	21.7	26.7	−0.623
5040	53258.924	28.7	0.092	7.10	(+22.6 ∼ −5.04)	33.6	27.3	−0.785
5955	53457.553	28.7	0.002	65.7	(+80.3 ∼ +49.1)	39.2	−26.5	0.000

TABLE 2
Wavelength ranges selected for Doppler measurement

No.	Range λ (Å)	Selected Emission lines (λ_{lab})
	for HEG and MEG	
1	6.0 – 6.50	Si XIV λλ6.1804, 6.1858
2	6.6 – 6.72	Si XIII λλ6.6479, 6.6882
3	8.3 – 8.55	Mg XII λλ8.4192, 8.4246
4	9.12 – 9.35	Mg XI λλ9.1687,9.2312,9.3143
	...	Fe XXI λ9.1944
5	12.00 – 12.20	Ne X λλ12.132, 12.137
	...	Fe XVII λ12.124
6	14.9 – 15.1	Fe XVII λ15.014
	...	Fe XIX λ15.079
	for MEG only	
7	18.85 – 19.1	O VIII λλ18.967,18.988
8	21.4 – 22.2	O VII λλ21.602,21.804,22.098
9	24.5 – 25.1	N VII λλ24.779,24.785

the $\pm 1^{st}$ orders of the HEG and MEG spectra separately; and then (3) calculate this region's Doppler velocity. The average value of these velocities from spectral segments and grating orders was taken to be the apparent Doppler velocity of Capella for the observation.

Despite the high spectral resolution obtained with the HETGS, almost all of the observed emission lines are blended (e.g., all hydrogenic lines are a blend originating from two transitions to the ground state, 1s $^2S_{1/2}$, from 2p $^2P_{3/2}$ and 2p $^2P_{1/2}$ states). Such an unresolved line complex was modeled as a blend in order to make a precise measurement of its apparent Doppler shift. For the baseline spectral model, a three-temperature *APED* plasma model[4] was chosen to represent the Capella spectrum (similar to the model used in Canizares et al. 2000). The three temperatures were fixed (at $kT \sim 10^{6.3}$, $10^{6.8}$, and $10^{7.1}$). The three free parameters, the normalization of line emission and the apparent Doppler velocity and width, were then fit by minimizing the C-statistic using the Levenberg-Marquardt method as implemented in ISIS version 1.3.0 (Houck & Denicola 2000). All quoted errors in the Doppler velocity term correspond to 3σ confidence levels (see the fifth and sixth columns in Table 1).

The regions were selected to include bright emission lines; the selected spectral regions and emission lines included in the fitting process are tabulated in Table 2. Once all the measurements were done, we took all of the velocities per wavelength region per grating, rejected the highest and lowest (i.e., *possibly anomalous*) data points, and then took the mean as the apparent velocity of the system. The measured Doppler widths were small and statistically insignificant ($\leq$150 km s^{-1}).

Each measurement of apparent Doppler velocity needed to be corrected for the barycentric motion of the Earth around the center of mass of the Solar system. The barycentric correction was made using the algorithm of Stumpff (1980) . Although we also applied the correction for the motion of the spacecraft, it turned out to be insignificant for our analysis. Even at its maximum, the scale was less than 1 km s^{-1} for Capella's location on the sky. Barycenter-corrected radial velocities V_{bary} are derived as:

$$V_{bary} = V_{obs} + C_{bary} + C_{sc}$$

where V_{obs} is the measured apparent Doppler velocity, C_{bary} and C_{sc} are the barycentric correction and the correction for the motion of the spacecraft, respectively.

4. DETECTION OF THE DOPPLER MOTION OF CAPELLA

Figure 1 shows the apparent radial velocities of Capella measured without barycentric correction. The data points are seemingly randomly scattered, though close comparison with the calculated apparent radial motion of *the primary Capella Aa* (the dashed curve) indicates that the observed hard X-ray emission lines of Capella trace the primary star's motion. The zero orbital phase of the Capella system applied in this work is defined by Hummel et al. (1994) as

$$P_0(n) = JD2447528.45(\pm 0.02) + 104.022 \times n$$

where n is an integer. Other orbital parameters are defined as follows: the orbital inclination $i = 137.18°$, ec-

[4] *APED* is a model for collisionally excited thermal plasma (Smith et al. 2001).

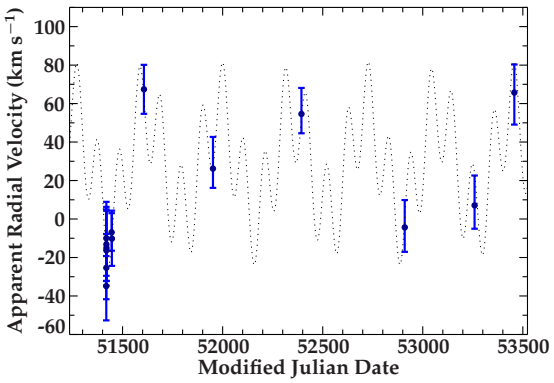

FIG. 1.— Apparent radial velocities of Capella measured with the Chandra/HETGS. The dotted line shows the calculated apparent radial motion of Capella Aa viewed from Earth (including the Barycentric, orbital and systemic motion of Capella Aa). 3σ error bars are shown in the plot.

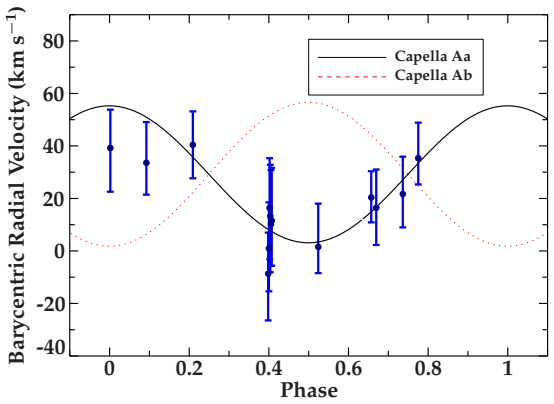

FIG. 2.— The observed radial motion of Capella vs. orbital phase after barycentric correction (see the 7th column in Table 1). The measured radial velocity clearly follows the trend of Capella Aa (primary). 3σ error bars are shown in the plot.

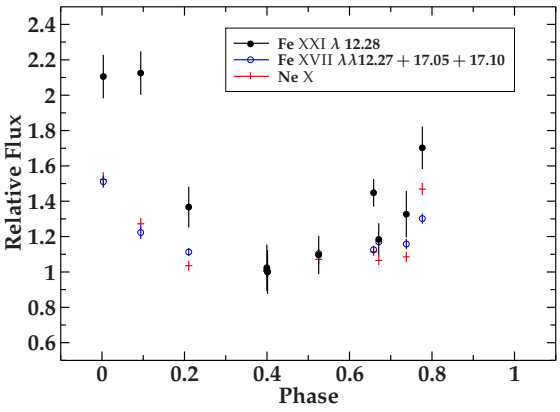

FIG. 3.— Changes in relative integrated line flux of hot (Fe XXI; filled circle) and cool (three Fe XVII and Ne X; open circle and cross) emission lines. The measured line fluxes are scaled relative to the lowest flux observed near phase = 0.4. 1σ error bars are shown in the plot.

centricity $e = 0.0$, the masses of the primary and companion stars $M_p = 2.69\ M_\odot$ and $M_s = 2.56\ M_\odot$, the node of ascension $\Omega(2000.0) = 40.8°$, the velocity amplitudes K_1 and K_2 for the primary and secondary stars are 26.05 and 27.40 km s^{-1}, and the systemic velocity[5]

[5] the systemic velocity γ and velocity amplitudes K_1 and K_2 are quoted from Barlow et al. (1993).

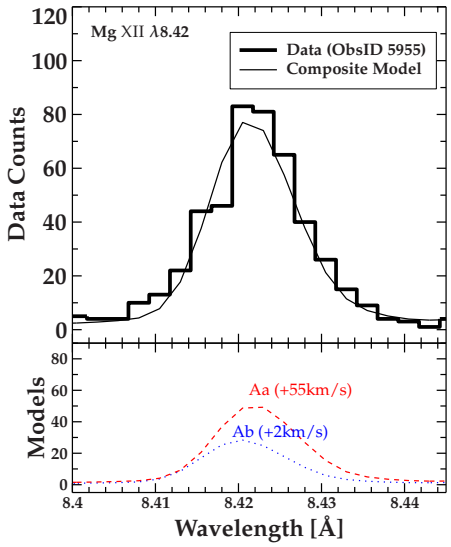

FIG. 4.— Two-velocity-component fit to the Mg XII blend at 8.42Å. At the phase = 0.002 (ObsID 5955), barycenter-corrected radial velocities for Capella Aa and Ab are expected to be 55 and 2 km s^{-1}, respectively. With the line positions fixed, the ratio of the normalization terms for Capella Aa and Ab is then derived to be roughly 2 : 1.

$\gamma = 29.20$ km s^{-1}. In Figure 2, the same data points were barycenter corrected and mapped into and plotted versus orbital phase. The velocity vs. phase diagram makes it clearer that the X-ray emission lines detected with the *Chandra*/HETGS closely trace the motion of Capella's primary star, as opposed to the secondary.

5. COMMENTS ON SCIENCE AND CALIBRATION

In six years of monitoring Capella, the *Chandra*/HETGS data reveal that the Doppler shifts of the bright X-ray emission lines closely follow the primary star of the Capella system. This implies that the G8 III primary star has been the dominant X-ray source of 10^7 K plasma, at least, in the last six years.

The identity of the dominant source of hot plasma in the Capella system has been somewhat controversial. It was long suspected that the G8 giant was responsible for the hard X-ray plasma, since the secondary star belongs to the class of X-ray deficient stars (late F – early G giants; see Ayres et al. 1998). This view is strongly supported by a *Far Ultraviolet Spectroscopic Explorer* observation of Capella, which concluded that the far UV Fe XVIII λ974.85 flux (formed at $10^{6.8}$ K) originated solely from the G8 star's corona (Young et al. 2001). The evidence pointing to the slower-rotating G8 star as the dominating source of coronal emission is particularly interesting, considering that the G1 star appears to dominate the UV emission formed at lower temperatures ($T < 10^6$ K in the transition region and chromosphere; see Woods & Ayres 1995 and Linsky et al. 1995). On the contrary, the detection of strong Fe XXI λ1354 (formed at 10^7 K) far-UV emission from the G1 star with the *HST*/STIS by Johnson et al. implies that the G1 giant might have dominated the hotter plasma (c.f. Linsky et al. 1998). Variability in luminosity is another issue for concern, as Capella (notably the G8 component) is known to vary in the hottest UV emission lines (Fe XXI to XXIV; see Brickhouse et al. 2000 and

Ayres et al. 2003). In X-rays, however, it is considered to be a steady source with no prior detection of flares (e.g., see Argiroffi et al. 2003). Is it then reasonable to infer that the two giants in Capella are remarkably steady X-ray sources? Light curves of Fe and Ne emission lines in Figure 3 illustrate that this is not necessarily the case. Based on the integrated line fluxes measured in Fe XXI λ12.28, three Fe XVII $\lambda\lambda$12.27+17.05+17.10, and Ne X Lyα λ12.13 lines, it appears that the line flux from the cooler plasma (i.e., Fe XVII and Ne X lines) changes by 20 – 50% over time, while the hottest emission line (Fe XXI) is more modulated (by a factor of two) than the cooler counterpart.

Furthermore, the two largest modulations of Fe XXI in line flux were observed in the last two observations of Capella (MJD = 53258.924 and 53457.553, or phase = 0.092 and 0.002, respectively). Examining Figure 2 closely, we notice that these two barycentric radial velocities are significantly lower than expected. It is suggestive that the deviation of the last two data points is probably due to an increasing level of contamination by the secondary's line emission flux originating from hot 10^7 K plasma. This scenario is supported by the observed characteristics of thermal distribution of plasma in single giants analogous to the components of Capella. The clump K0 giant β Cet, analogous to Capella Aa, shows a thermal distribution sharply peaked at $T \sim 10^{6.8}$ K (Ayres et al. 1998); on the other hand, the Hertzsprung gap G0 giant 31 Com, analogous to Capella Ab, is characterized instead by a temperature distribution steeply increasing up to the 10^7 K peak temperature and a large amount of plasma at even hotter temperatures (Scelsi et al. 2004). Assuming that the Capella components have analogous thermal structures, it is then reasonable to assume that the G8 star is the stronger X-ray source, but the G1 star significantly contributes to the hotter emission at $T \gtrsim 10^7$ K. Figure 4 shows that *indeed* bright and isolated Mg XII Lyα doublets can be fit well with two line components associated with Capella Aa and Ab. In the lower panel of Figure 4, the dashed line centered at barycenter-corrected radial Doppler velocity +55 km s^{-1} is the Mg XII doublets from Capella Aa (G8 III) and the dotted line centered at +2 km s^{-1} is the same doublets from Capella Ab (G1 III). The composite of the two models is shown as the solid line in the top panel of Figure 4. In this preliminary analysis, the intrinsic line widths for both components were set to zero. To quantify the velocity perturbation in terms of how much flux would be required from the secondary star to offset the radial velocity, the normalization terms for each line component were allowed to vary. The best fit resulted from the line flux ratio (G8/G1) of 1.8 : 1 in the Mg XII feature. The weighted mean for the two Doppler velocities is $(55\ km/s \times 1.8 + 2\ km/s)/(1.8+1) = 36.1\ km/s$, which is reasonably close to the measured radial velocity of 39.2 km s^{-1} (see Table 1). This finding indicates that the secondary star may have contributed as much as one third of the flux in the HETGS wave-band during the observations for ObsID 5040 and 5955. This analysis of variation in integrated line flux is still very preliminary and a further discussion is deferred to a future publication.

Lastly we find that the *Chandra*/HETGS appears to be a very stable instrument in the long run. The improvements in the ACIS-S geometry values and the MEG grating period (provided in CALDB 3.0.1, version `geomN0005`) further enhance its capability to detect a miniscule dynamic motion of an astrophysical source. The differences between the measured and expected Doppler velocity of Capella Aa generally lie under 20 km s^{-1}, which we shall consider as the systematic uncertainty in Doppler velocity determination using the entire coverage of the HETGS. As for absolute wavelength determination (i.e., per emission line), inspection of our detailed fits indicates that the *r.m.s.* of the differences derived per emission line are 25 and 33 km s^{-1} with the HEG and MEG, respectively.

We would like to thank our referee for his insightful comments on this letter. We are also grateful for technical support provided by J. E. Davis and J. Houck at MIT. This research was supported by NASA through the SAO contract SV3-73016 to MIT for support of the Chandra X-Ray Center and Science Instruments, operated by SAO for and on behalf of NASA under contract NAS8-03060.

Facilities: CXO (HETGS)

REFERENCES

Argiroffi, C., Maggio, A., & Peres, G. 2003, A&A, 404, 1033
Ayres, T., R., Brown, A., Harper, G. M., Osten, R. A., Linsky, J. L., Wood, B. E., & Redfield, S. ApJ, 583, 963
Ayres, T., R., Simon, T., Stern, R. A., Drake, S. A, Wood, B. E., & Brown, A. 1998, ApJ, 496, 428
Barlow, D. J., Fekel, F. C., & Scarfe, C. D. 1993, PASP, 105, 476
Brickhouse, N. S., Dupree, A. K., Edger, R. J., Liedahl, D. A., Drake, S. A., White, N. E., & Singh, K. P. 2000, ApJ, 530, 387
Canizares, C. R., Davis, J. E., Dewey, D., Flanagan, K. A., Galton, E. B., Huenemoerder, D. P., Ishibashi, K., Markert, T. H., Marshall, H. L., McGuirk, M., Schattenburg, M. L., Schulz, N. S., Smith, H. I., & Wise, M. 2005, PASP, 117, 1144.
Canizares, C. R., Huenemoerder, D. P., Davis, D. S., Dewey, D., Flanagan, K. A., Houck, J., Markert, T. H., Marshall, H. L., Schattenburg, M. L., Schulz, N. S., Wise, M., Drake, J. J., & Brickhouse, N. S. 2000, ApJ, 539, L41
Houck, J. C., & Denicola, L. A. 2000, in ASP Conf. Ser. 216, Astronomical Data Analysis Software and Systems IX, ed. N. Manset, C. Veillet, & D. Crabtree (San Francisco: ASP), 591
Hummel, C. A., Armstrong, J. T., Quirrenbach, A., Buscher, D. F., Mozurkewich, D., & Elias II, N. M. 1994, AJ, 107, 1859
Johnson, O., Drake, J. J., Kashyap, V., Brickhouse, N. S., Dupree, A. K., Freeman, P., Young, P. R., & Kriss, G. A. 2002, ApJ, 565, L97
Linsky, J. L., Wood, B. E., Brown, A., & Osten, R. A. 1998, ApJ, 492, 767
Linsky, J. L., Wood, B. E., Judge, P., Brown, A., Andrulis, C., & Ayres, T. R. 1995, ApJ, 442, 381
Ness, J.-W., Brickhouse, N. S., Drake, J. J., & Huenemoerder, D. P. 2003, ApJ, 598, 1277
Pilachowski, C. A. & Sowell, J. R. 1992, AJ, 103, 1668
Scelsi, L., Maggio, A., Peres, G., & Gondoin, Ph. 2004, A&A, 413, 643
Smith, R. K., Brickhouse, N. S., Liedahl, D. A., & Raymond, J. C. 2001, ApJ, 556, L91
Stumpff, P. 1980, A&A Suppl., 41, 1
Wood, B. E. & Ayres, T. R. 1995, ApJ, 443, 329
Young, P. R. & Dupree, A. K. 2002, ApJ, 565, 598
Young, P. R., Dupree, A. K., Wood, B. E., Redfield, D., Linsky, J. L., Ake, T. B., & Moos, H. W. 2001, ApJ, 555, L121